*Research Article*

MOLECULAR PAIN

Molecular Pain
Volume 14: 1–15

DOI: 10.1177/1744806918814640
journals.sagepub.com/home/mpx
SAGE

# Differential modulation of voltage-gated sodium channels by nerve growth factor in three major subsets of TrkA-expressing nociceptors

**Irina Schaefer[1], Vincenzo Prato[1], Alice Arcourt[1,2], Francisco J Taberner[1], and Stefan G Lechner[1]**

## Abstract

Nerve growth factor is an inflammatory mediator that induces long-lasting hyperalgesia, which can partially be attributed to nerve growth factor-induced sensitization of primary afferent nociceptors. It was shown that nerve growth factor increases the excitability of polymodal C-fibre nociceptors by modulating tetrodotoxin-sensitive and tetrodotoxin-resistant voltage-gated sodium channels, but hitherto only little is known about the effects of nerve growth factor on sodium currents in other nociceptor subtypes that express the nerve growth factor receptor TrkA. We previously characterized two reporter mouse lines that allow the unequivocal identification of two important subclasses of TrkA-expressing nociceptors – i.-e. neuropeptide Y receptor type 2 ($NPY2R^+$) A$\delta$-fibre nociceptors that mediate pinprick pain and nicotinic acetylcholine receptor alpha-3 subunit ($CHRNA3^+$) silent nociceptors, which are the most abundant $TrkA^+$ nociceptors in visceral organs and deep somatic tissues. Here, we utilized these mouse lines to investigate the expression patterns and the possible nerve growth factor-dependent modulation of sodium channels in these neurons using whole-cell patch-clamp recordings and quantitative real-time polymerase chain reaction. We demonstrate that $NPY2R^+$ nociceptors, $CHRNA3^+$ 'silent' nociceptors and polymodal C-fibre nociceptors express different combinations of sodium channel $\alpha$- and $\beta$-subunits and accordingly exhibit functionally different sodium currents. Moreover, we demonstrate that nerve growth factor produces robust hyperpolarizing shifts in the half-activation voltage of tetrodotoxin-resistant currents in $NPY2R^+$ nociceptors and polymodal C-fibre nociceptors and also shifts the half-activation of tetrodotoxin-sensitive currents in polymodal C-fibre nociceptors. In silent nociceptors, however, nerve growth factor solely increases the current density of the tetrodotoxin-resistant current but does not alter other sodium channel properties. Considering the different peripheral target tissues and the previously reported roles in different forms of pain of the nociceptor subpopulations that were examined here, our results suggest that nerve growth factor differentially contributes to the development visceral and cutaneous pain hypersensitivity and highlights the importance of developing different therapeutic strategies for different forms of pain.

## Keywords

Voltage-gated sodium channel, nerve growth factor, pain, hyperalgesia, A-fibre nociceptor, silent nociceptor, peripheral sensitization

Date Received: 1 August 2018; revised: 28 September 2018; accepted: 16 October 2018

## Introduction

Nerve growth factor (NGF) is not only a neurotrophic factor that is important for the embryonic development of the sympathetic and sensory nervous system, but it is also a potent inflammatory mediator that plays a crucial role in the development and maintenance of chronic inflammatory pain.[1,2] Thus, the NGF levels are

[1]Institute of Pharmacology, Heidelberg University, Heidelberg, Germany
[2]Centre for Developmental Neurobiology, King's College London, London, UK

**Corresponding Author:**
Stefan G Lechner, Institute of Pharmacology, Heidelberg University, Im Neuenheimer Feld 366, 69120 Heidelberg, Germany.
Email: stefan.lechner@pharma.uni-heidelberg.de

increased in inflamed tissues in several human pain disorders including interstitial cystitis,[3] irritable bowel syndrome,[4] chronic pancreatitis[5] and osteoarthritis,[6] and administration of NGF produces profound and long-lasting thermal and mechanical hyperalgesia in rodents and humans.[7–11] Accordingly, antibodies that block NGF signalling by sequestering endogenously produced NGF, have proven great efficacy in alleviating pain in rodents[12] and, most importantly, in humans suffering from the aforementioned pain disorders.[1,13]

The cellular and molecular basis of NGF-induced thermal hyperalgesia is well understood, but only little is known about the mechanism underlying mechanical hyperalgesia.[2] Thus, thermal hyperalgesia results from the sensitization of the heat and capsaicin-sensitive ion channel TRPV1 in polymodal C-fibre nociceptors.[14–16] Regarding mechanical hyperalgesia, both, central as well as peripheral sensitization, mechanisms have been proposed to be involved.[1,2] Central sensitization is thought to be, at least partially, mediated by an NGF-induced increase in brain-derived neurotrophic factor release from the central terminals of nociceptors, which causes a strengthening of synaptic transmission between nociceptors and second-order neurons in the spinal dorsal horn via modulation of post-synaptic N-methyl-D-aspartic acid receptors.[17]

Peripheral sensitization, that is increased sensitivity of nociceptive primary afferents to noxious mechanical stimuli, is thought to result from a combination of alterations of different functional properties of nociceptors. One possibility is that the yet unknown ion channels that mediate mechanotransduction in nociceptors – i.e. the conversion of noxious mechanical stimuli into electrical signals – are sensitized by NGF, such that a given mechanical stimulus causes a larger depolarization of the peripheral sensory endings and hence elicits more action potentials. Indeed, it was shown that mechanotransduction currents in small diameter nociceptors are sensitized by direct activation of protein kinase C or treatment with a mixture of the inflammatory mediators bradykinin, prostaglandin $E_2$, histamine and serotonin, only when the cells are pre-exposed to NGF.[18,19] Moreover, we have recently shown that a subset of peptidergic nociceptors that are characterized by the expression of the alpha-3 subunit of the nicotinic acetylcholine receptor (CHRNA3) and that are normally completely insensitive to mechanical stimuli becomes mechanosensitive following treatment with NGF.[19] Considering that $CHRNA3^+$ nociceptors account for almost half of all peptidergic nociceptors in visceral organs, muscles and joints,[19] it is tempting to speculate that the NGF-induced un-silencing of these afferents would greatly increase nociceptive input to projection neurons in the spinal dorsal horn and may thus significantly contribute to mechanical hyperalgesia.

In addition to mechanotransduction channels, voltage-gated sodium channels (VGSCs) are also major determinants of nociceptor sensitivity as they set the action potential threshold and the maximum firing frequency. Accordingly, modulation of VGSCs might also significantly contribute to mechanical hyperalgesia.[20,21] Nociceptors predominantly express four of the nine known isoforms of VGSC alpha subunits, namely, the tetrodotoxin-sensitive (TTX-S) isoforms $Na_v1.6$ and $Na_v1.7$ as well as the TTX-resistant (TTX-R) isoforms $Na_v1.8$ and $Na_v1.9$.[20,21] NGF was shown to modulate voltage-gated sodium currents via both transcriptional regulation as well as post-translational modifications.[1,2,20,21] Thus, NGF was shown to increase the current density and to cause a hyperpolarizing shift in the voltage dependence of activation of $Na_v1.8$. The former effect appears to require p38 mitogen-activated protein (MAP) kinase,[22] whereas the latter is mediated by a signalling cascade that involves the second messenger ceramide and the atypical protein kinase PKMζ.[23,24] The increase in current density is commonly attributed to an NGF-induced upregulation of $Na_v1.8$, but in fact there is only indirect evidence for this hypothesis and the reports regarding this matter are somewhat conflicting. Thus, while some studies show that NGF reverses axotomy-induced downregulation of $Na_v1.8$[25,26] and that in-vivo NGF deprivation causes a downregulation of $Na_v1.8$,[27] other found no differences in the expression of $Na_v1.8$ in dorsal root ganglion (DRG) neurons isolated from animals in which hyperalgesia had been induced with NGF.[28,29] $Na_v1.7$ expression was also shown to be upregulated by NGF[29] and there is indirect evidence suggesting that NGF might also shift the voltage dependence of activation of $Na_v1.7$ to more negative potentials, because ERK1/2 MAP kinase, which is a downstream target of NGF-TrkA signalling, was shown to do so in heterologous systems.[30]

Most of the above-mentioned studies that investigated the modulation of VGSCs by NGF in DRG cultures using whole-cell patch-clamp recordings have focused on polymodal C-fibre nociceptors that express the NGF receptor TrkA, because these neurons can readily be identified in cultures as small diameter cells that are not labelled by Isolectin B4 (IB4) and respond to the TRPV1 agonist capsaicin.[1,21] The TrkA receptor is, however, also expressed by other nociceptor subpopulations, but the lack of tools that would allow the unequivocal identification of these subpopulations in DRG cultures has hitherto precluded the thorough examination of the effects of NGF on sodium currents in these physiologically important nociceptor subtypes. We have recently generated a mouse line in which enhanced yellow fluorescent protein (EYFP)-tagged Channelrhodopsin 2 is exclusively expressed in sensory neurons that express the neuropeptide Y receptor type 2

(NPY2R). We showed that NPY2R$^+$ neurons are myelinated TrkA$^+$ Aδ-fibre nociceptors and demonstrated that these nociceptors are required for the detection of pinprick stimuli.[31] Moreover, as mentioned earlier, we have recently characterized a reporter mouse line in which green fluorescent protein (GFP) is expressed in CHRNA3$^+$ neurons and demonstrated that these neurons constitute TrkA$^+$ 'silent' C-fibre nociceptors.[19]

Here, we utilized the NPY2R and CHRNA3 reporter mouse lines to investigate the modulation of voltage-gated sodium currents by NGF in Aδ-fibre nociceptors and silent nociceptors in DRG cultures, using whole-cell patch-clamp recordings and quantitative real-time polymerase chain reaction (qRT-PCR).

## Materials and methods

### Animals

CHRNA3-EGFP mice, official name Tg(Chrna3-EGFP) BZ135Gsat/Mmnc (RRID:MMRRC_000243-UNC) and Npy2r$^{Cre/+}$, official name Tg(Npy2r-cre)SM19Gsat/Mmucd (RRID:MMRRC_036630-UCD) and ChR2$^{loxP/+}$ animals (B6;129S-Gt(ROSA)26Sortm32(CAG-COP4*H134R/EYFP)Hze/J; RRID:IMSR_JAX:012569) were obtained from Jackson Laboratories. Mice were housed in the Interfacultary Biomedical Facility of Heidelberg University according to the institutional guidelines, and all animal experiments were carried out according to the German Animal Protection Law and with permission of the Regierungspraesidium Karlsruhe (T-57/16).

### DRG cell culture

Twelve to eighteen weeks old female mice were killed by placing them in a $CO_2$-filled chamber for 2 to 4 min followed by cervical dislocation. L2–L5 DRGs were collected in $Ca^{2+}$ and $Mg^{2+}$-free phosphate-buffered saline (PBS) and incubated in a mixture of Collagenase type I (2.0 μg/ml, Sigma) and Trypsin (1.5 μg/ml, Sigma) for 60 min at 37°C. Digested DRG's were washed twice with growth medium (Dulbecco's modified Eagle's medium-F12 (Invitrogen) supplemented with L-glutamine (2 μM, Sigma), glucose (8 mg/ml, Sigma), penicillin (200 U/ml)–streptomycin (200 μg/ml) (both Life Technologies) 5% fetal horse serum (Life Technologies)), triturated with a fire-polished Pasteur pipette and plated in a droplet of growth medium on glass coverslips precoated with poly-L-lysine (20 μg/cm$^2$, Sigma) and laminin (4 μg/cm$^2$, Life Technologies). To allow neurons to adhere, the coverslips were kept for 3 to 4 h at 37°C in a humidified 5% incubator before being flooded with fresh growth medium. Cultures were used for patch-clamp experiments on the next day.

### Immnuohistochemistry

DRGs were dissected in ice-cooled PBS, fixed with 4% paraformaldehyde for 30 min at 4°C and incubated overnight in 30% sucrose at 4°C. DRGs were then embedded in Tissue-Tek O.C.T compound and cut into 16 μm cryo-sections. After drying, sections were incubated in 50 mM Glycine for 20 min, washed twice with PBS with Tween 20 (PBST) (0.2%), blocked with PBST (0.2%) + 10% donkey serum + 1% bovine serum albumin and then incubated with primary antibodies for 1 h at room temperature (RT). Primary antibodies were diluted in PBST (0.2%) + 10% donkey serum. Sections were then washed four times with PBST (0.2%), subsequently incubated with secondary antibodies for 1 h at RT, washed with PBST four times, dried and mounted with fluorogel (Fluoprobes).

### Antibodies

The following primary antibodies were used: rat anti-GFP (Nacalai tesque, #04404–84, 1:3000; RRID: AB_10013361), mouse anti-neurofilament heavy polypeptide (NEFH) (Sigma-Aldrich, N0142, 1:600, RRID: AB_477257), goat anti-TrkA (R&D, AF1056, 1:200, RRID:AB_2283049) and Isolectin GS-IB4-Alexa Fluor® 568 Conjugate (Life technologies, 3 μg/ml). Secondary antibodies were AlexaFluor-488 donkey anti-rat (Life technologies, AF21208, 1:500, RRID: AB_2535794), AlexaFluor-594 donkey anti-mouse (Life technologies, AF21203 1:500, RRID:AB_2535789) and AlexaFluor-633 donkey anti-goat (Life technologies, A21082, 1:500, RRID:AB_10562400).

### Electrophysiology

Whole-cell patch-clamp recordings were made at RT (20–24°C). Patch pipettes with a tip resistance of 0.8 to 1.5 MΩ were pulled (Flaming-Brown puller, Sutter Instruments, Novato, CA, USA) from borosilicate glass capillaries (BF150-86–10, Sutter Instrument), filled with a solution consisting of 120 mM CsCl, 10 mM NaCl, 20 mM TEA-Cl, 1 mM 4-aminopyridine, 1 mM EGTA, 10 mM HEPES, 2 mM guanosine 5′-triphosphate (GTP) and 2 mM adenosine 5′-triphosphate (ATP) adjusted to pH 7.3 with CsOH. The bathing solution contained 144 mM NaCl, 2 mM $CaCl_2$, 1 mM $MgCl_2$, 4 mM glucose, 10 mM HEPES and 100 μM $CdCl_2$ adjusted to pH 7.4 with NaOH. TTX and capsaicin were applied with a gravity-driven multi-barrel perfusion system (Valvelink8.2, Automate Scientific). All recordings were made using an EPC-10 amplifier (HEKA, Lambrecht, Germany) in combination with Patchmaster© and Fitmaster© software (HEKA). Pipette and membrane capacitance were compensated using the auto function of Patchmaster, and series

resistance was compensated by >70% to minimize voltage errors. Using this approach, the maximal voltage errors shown in Table 1 for TTX-S and TTX-R currents were achieved.

Currents were sampled at 20 kHz, filtered at 2.9 kHz and linear leak currents were subtracted using a P/4 pulse protocol. Whole-cell sodium currents were elicited by a series of 40 ms step depolarizations from a holding potential of −120 mV to test potentials ranging from −70 mV to +60 mV in increments of 5 mV at an interval of 1 s. The TTX-S currents were isolated by subtracting the current recorded in the presence of 300 nM TTX (TTX-R current) from the total current recorded in the absence of TTX. For conductance–voltage curves, $Na^+$ conductance (G) was calculated was calculated using the following equation: $G = I_{Na}/(V\text{-}E_{Na})$, where $I_{Na}$ is the peak current amplitude at the test potential V, and $E_{Na}$ is the reversal potential of sodium (+62.9 mV), which was calculated with the Nernst equation. To determine the voltage at which half of the sodium channels are activated ($V_{1/2}$), $G/G_{max}$ curves were fit with a Boltzmann equation: $G/G_{max} = 1/[1+\exp(V_{1/2}-V/k)]$, where $G_{max}$ is the maximal conductance, V is the test potential and k is the slope factor.

## Fura2-$Ca^{2+}$ imaging

To identify peptidergic C-fibre nociceptors – i.e. $IB4^-$ neurons that respond to the TRPV1 agonist capsaicin – for the collection of cell samples for qRT-PCR, FURA-2-$Ca^{2+}$ imaging was used. To this end, cultured DRG neurons loaded with FURA-2 (25 μM) and labelled with 1.5 μg/ml Isolectin GS-IB4-Alexa Fluor 568 conjugate at 37°C for 25 min and then washed with PBS for 10 min. Neurons were placed in a chamber containing extracellular buffer consisting of 140 mM NaCl, 1 mM $MgCl_2$, 2 mM $CaCl_2$, 4 mM KCl, 4 mM glucose and 10 mM HEPES adjusted to pH 7.4. Cells were illuminated alternately at 340 nm and 380 nm (100 ms exposure time Polychrome V, Visitron Systems) at a sampling frequency of 2 Hz, and Fura-2 fluorescence images were acquired with a ProgRes $MF^{Cool}$ charge-coupled device (CCD) camera (Jenoptik, Germany). The Polychrome V and the ProgRes $MF^{Cool}$ CCD camera were controlled by the imaging extension of the PatchMaster software (HEKE Elektronik). Fura-2 ratio images were generated with the ImageJ software. Neurons with a cell soma diameter <25 μm that were not labelled by IB4 and exhibited an increase in the Fura-2 signal in response to capsaicin were considered as peptidergic polymodal C-fibre nociceptors. To ensure that we did not collect silent nociceptors, some of which are also small and respond to capsaicin, all $IB4^-/caps^+$ neurons were collected from cultures prepared from $CHRNA3^{EGFP}$ mice and the lack of a GFP signal was used as an additional selection criterion.

## Cell sample collection and qRT-PCR

mRNA expression levels of VGSCs and beta subunits were determined as follows. From each nociceptor subpopulation ($CHRNA3^+$, $NPY2R^+$ or $IB^-/caps^+$) and each treatment condition (control and NGF), four cell samples (20 cell per sample) were collected from DRG cultures by aspirating the cells into a patch-clamp pipette with a tip diameter of 25 μm, filled with 2 to 4 μl PBS containing 4 U/μl RNAseOUT (Thermofisher). cDNA synthesis was carried out directly on the sample using the Power SYBR® Green Cells-to-CT™ Kit (Life Technologies) according to the manufacturers' instructions. qRT-PCR reactions were set up using FastStart Essential DNA Green Master (Roche) by adding 4 μL of the obtained cDNA as template, and the primer pairs mentioned in Table 2 were used at a concentration of 250 nM.qRT-PCR reactions were performed in a LightCycler 96 (Roche) with a thermal cycler profile as follows: 10 min preincubation step at 95°C followed by 40 cycles of PCR with a 10 s denaturing cycle at 95°C, followed by 10 s of annealing at 60°C and 10 s extension at 72°C.

## Statistics

All statistical analyses were made using GraphPad Prism 7. The statistical tests that were used are mentioned in the figure legends and in the main text.

**Table 1.** Summary of patch-clamp recording parameters.

| Cell population | Access resistance (mean ± SEM) | Compensation (%) | Maximum voltage error TTX-S (mV) | Maximum voltage error TTX-R (mV) |
|---|---|---|---|---|
| $CHRNA3^+$ (ctl) | 3.1 ± 0.37 | 80.1 ± 2.4 | 6.7 ± 1.6 | 3.3 ± 0.8 |
| $CHRNA3^+$ (NGF) | 2.9 ± 0.39 | 78.9 ± 2.1 | 9.6 ± 1.7 | 5.3 ± 1.6 |
| $NPY2R^+$ (ctl) | 2.9 ± 0.22 | 87.8 ± 0.7 | 8.8 ± 1.4 | 2.6 ± 0.3 |
| $NPY2R^+$ (NGF) | 2.5 ± 0.27 | 87.9 ± 0.5 | 7.1 ± 1.2 | 4.0 ± 0.7 |
| $IB4^-/caps^+$ (ctl) | 4.2 ± 1.21 | 76.2 ± 0.9 | 4.7 ± 1.3 | 2.2 ± 0.3 |
| $IB4^-/caps^+$ (NGF) | 3.9 ± 0.82 | 81.4 ± 3.1 | 4.1 ± 1.6 | 1.6 ± 0.4 |

NGF: nerve growth factor; IB4: Isolectin B4; NPY2R: neuropeptide Y receptor type 2; CTL: control.

**Table 2.** List of primers used for qRT-PCR.

| | |
|---|---|
| Nav1.6_ FWD | 5′-CAGCAGGTCGAGAAATGTCTTTC-3′ |
| Nav1.6_ REV | 5′- CTCAAGCATTTCTGCCATTTCC-3′ |
| Nav1.7_ FWD | 5′-GTGGGCGAATTCACCTTCCT-3′ |
| Nav1.7_ REV | 5′-TCGAAGAGCTGAAACATTGCCTA-3′ |
| Nav1.8_FWD | 5′-ATAAGGGGCCAGGACATCTTC-3′ |
| Nav1.8_REV | 5′-AAACACGAAGCCCTGGTACT-3′ |
| Nav1.9_FWD | 5′-TGAGGCAACACTACTTCACCAATG-3′ |
| Nav1.9_REV | 5′-AGCCAGAAACCAAGGTACTAATGATG-3′ |
| Beta1_ FWD | 5′-TGCATGATGGGTGAAGCAAT-3′ |
| Beta1_ REV | 5′-GCCTATGTGCAAATCAGCAAAA-3′ |
| Beta2_ FWD | 5′-ATACCCGCCTGCCCTGTACC-3′ |
| Beta2_ REV | 5′-TCTCCAAACCGCTCCAGCTTC-3′ |
| Beta3_ FWD | 5′-TATAAATGAGAAAGCCCTGGTTCTG-3′ |
| Beta3_ REV | 5′-GCCTAACCTAGTGCTCGACACA-3′ |
| Beta4_ FWD | 5′-GGATGCCCAAATGAGGGATT-3′ |
| Beta4_ REV | 5′-CCAGAGGACTAAACCATGCATAAGA-3′ |
| GAPDH- FWD | 5′-GCATGGCCTTCCGTGTTC-3′ |
| GAPDH-REV | 5′-GTAGCCCAAGATGCCCTTCA-3′ |

GAPDH: Glyceraldehyde 3-phosphate dehydrogenase.

N-numbers for each experiment – i.e. numbers of biological replicates – are provided in the figure or in the figure legend. To select the appropriate test, all data sets were tested for Gaussian distribution using the Kolmogorov–Smirnov test.

## Results

NGF exerts its effects via activation of the TrkA receptor, which is expressed in various functionally different subtypes of nociceptors including polymodal C-fibre nociceptors, mechanically insensitive 'silent' C-fibre nociceptors as well as myelinated Aδ-fibre nociceptors. Most of our current knowledge about the modulation of VGSCs by NGF is, however, limited to small diameter C-fibre nociceptors. Here, we have utilized two recently characterized reporter mouse lines that allow the unequivocal identification of silent nociceptors and Aδ-fibre nociceptors in DRG cultures in order to compare voltage-gated sodium currents and their possible modulation by NGF in all three subpopulations of $TrkA^+$ nociceptors. Since there is strong evidence for sex- and age-dependent differences in pain signalling both in mice and humans,[32,33] we only examined sensory neurons from fully matured (12–18 weeks old) female mice to ensure that these factors do not confound our results.

### *The properties of VGSCs differ between the three major subpopulations of $TrkA^+$ nociceptors*

To identify silent nociceptors, we prepared DRG cultures from CHRNA3-EGFP mice in which EGFP is exclusively expressed in this subset of nociceptors, which are unmyelinated as indicated by the lack of NEFH expression, have small-to-medium cell soma diameters and express the NGF receptor TrkA (Figure 1(a)).[19] Aδ-fibre nociceptors were visualized using $NPY2R^{ChR2}$ mice in which EYFP-tagged channelrhodopsin 2 expression is confined to myelinated $TrkA^+$ neurons with large cell bodies (Figure 1(b)), as previously described.[31] Finally, polymodal C-fibre nociceptors were identified in cultures from CHRNA3-EGFP mice as $EGFP^-/IB4^-$ small diameter neurons (< 25 μm) that were sensitive to capsaicin (Figure 1(c)).

Whole-cell sodium currents elicited by a series of 40 ms step depolarizations from −120 mV to test potentials ranging from −70 mV to +60 mV in increments of 5 mV were recorded before and after application of 300 nM TTX. The TTX-S currents were isolated by subtracting the TTX-R current from the total current recorded in the absence of TTX. The current–voltage relationship showed that TTX-S currents in $CHRNA3^+$ neurons and $NPY2R^+$ neurons activated at more hyperpolarized potentials than TTX-S currents in $IB4^-/caps^+$ nociceptors (Figure 1(a)) and revealed differences in current densities between the three nociceptor subpopulations (Figure 1(e)). Thus, the maximum current densities of the TTX-S currents in $NPY2R^+$ neurons were significantly bigger than the TTX-S current densities in the other two populations ($NPY2R^+$ $I_{max}$-TTX-S = $-1052 \pm 123.8$ pA/pF; $CHRNA3^+$: $I_{max}$-TTX-S = $450.2 \pm 112.4$ pA/pF; $IB4^-$/caps+: $I_{max}$-TTX-S = $-609.2 \pm 71.1$ pA/pF; Figure 1(e)). Boltzmann fits of the conductance–voltage relations shown in Figure 1 (f) revealed that the voltage for half-maximal activation ($V_{1/2}$) of TTX-S currents was significantly more negative in $CHRNA3^+$ ($V_{1/2} = -26.74 \pm 0.51$ mV) and $NPY2R^+$ ($V_{1/2} = -30.29 \pm 0.37$ mV) neurons as compared to $IB4^-/caps^+$ nociceptors ($V_{1/2} = -14.22 \pm 0.82$ mV) (Figure 1(g)). The TTX-R currents in the three nociceptor subpopulations (Figure 2(a)) also differed from one another in several aspects. Thus, the current densities of TTX-R currents were significantly bigger in $NPY2R^+$ nociceptors ($-272.7 \pm 30.4$ pA/pF) as compared to $CHRNA3^+$ neurons ($-188.4 \pm 21.7$ pA/pF) and $IB4^-/caps^+$ nociceptors ($-140.0 \pm 24.3$ pA/pF) (Figure 2(b) and (c)). Moreover, TTX-R currents in $CHRNA3^+$ neurons were activated at significantly more negative potentials ($V_{1/2} = -16.8 \pm 0.5$ mV) as compared to TTX-R currents in $NPY2R^+$ neurons, which had a $V_{1/2}$ of $-7.7 \pm 1.0$ mV, and $IB4^-/caps^+$ nociceptor with a $V_{1/2}$ of $-4.3 \pm 0.6$ mV (Figure 2(d) and (e)).

To test if the observed differences in current densities and in half-activation voltages of TTX-S and TTX-R currents (Figures 1 and 2) result from differences in the expression levels of certain VGSC α- and β-subunits, we next quantified the mRNA levels of $Na_v1.6$, $Na_v1.7$, $Na_v1.8$ and $Na_v1.9$, which are the most abundant α-subunit isoforms in DRG neurons, as well as the mRNA levels of the β1, β2, β3 and β4 subunits using qRT-PCR.

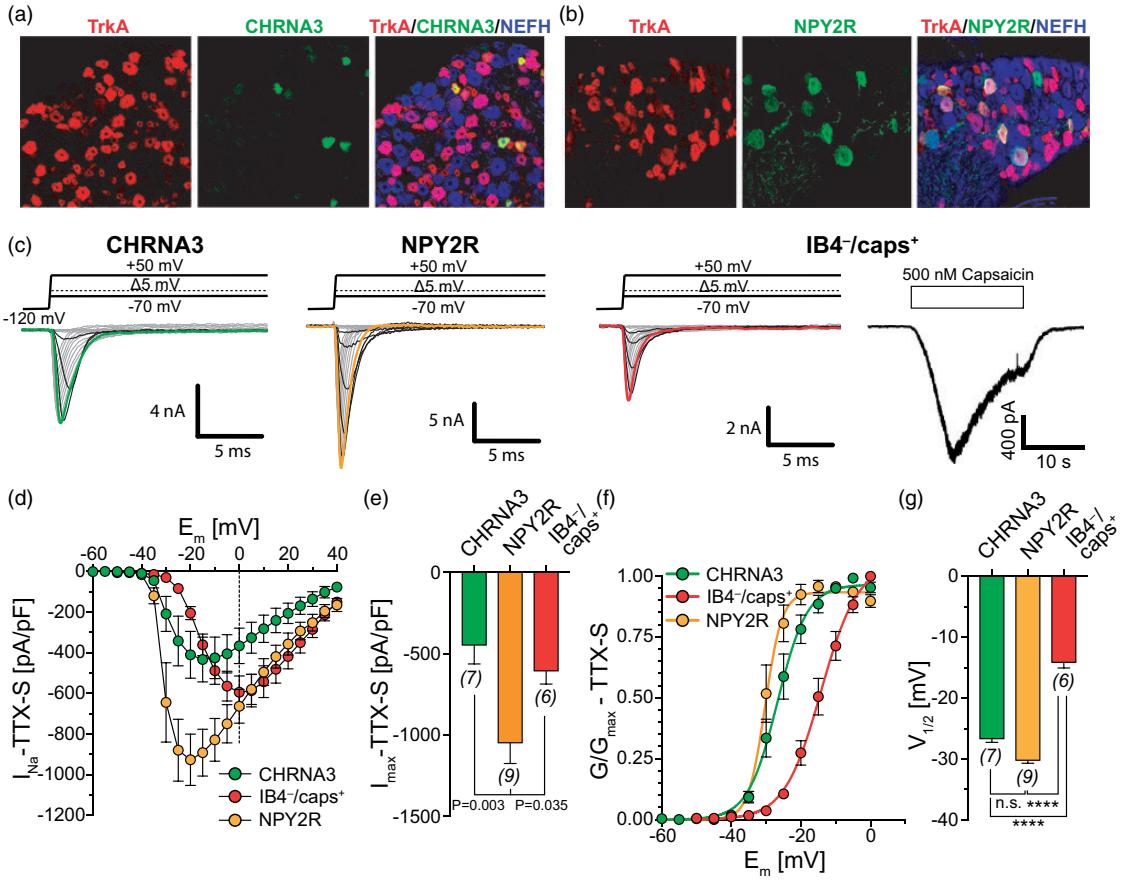


**Figure 1.** Differences in TTX-S sodium currents in three major subsets of TrkA-expressing neurons. (a) Immunohistochemistry of a DRG section showing that CHRNA3$^+$ neurons co-express the TrkA receptor but not NEFH. (b) Immunohistochemistry showing that NPY2R$^+$ neurons express both TrkA and NEFH. (c) Representative example traces of TTX-S currents (bottom traces) elicited by the indicated pulse protocol (top trace). The rightmost trace shows a typical response of a small diameter IB4$^-$ neuron to 500 nM capsaicin. (d) Current–voltage relationship of the TTX-S currents (mean current density ± SEM) in the indicated cell types. (e) Comparison of the current densities of the maximal TTX-S current in the indicated cell types using one-way ANOVA and Holm–Sidak's multiple comparison test. Note that the current densities of the TTX-S current were significantly bigger in NPY2R+ neurons as compared to the other two nociceptor subtypes. (f) Boltzmann fits of the conductance–voltage plots showing that TTX-S currents in NPY2R$^+$ and CHRNA$^+$ activate at more negative potentials compared to TTX-S currents in IB4$^-$ neurons. (g) Comparison of the $V_{1/2}$ ± SEM values obtained by the Boltzmann fits shown in (f). Boltzmann fits ($V_{1/2}$ values) were compared pairwise using the extra sum-of-squares F-test. ****$P < 0.0001$. TTX: tetrodotoxin; IB4: Isolectin B4; NPY2R: neuropeptide Y receptor type 2; NEFH: neurofilament heavy polypeptide; CHRNA3: nicotinic acetylcholine receptor alpha-3 subunit.

This analysis revealed that NPY2R$^+$ neurons express $Na_v1.6$ and the β-subunits β1 and β4 at significantly higher levels than IB4$^-$/caps$^+$ neurons (Figure 3(a)). Moreover, we observed a trend towards higher expression levels of $Na_v1.7$, $Na_v1.8$ and β2 in NPY2R$^+$ neurons as compared to IB4$^-$/caps$^+$ neurons, but these differences were not statistically significant (Figure 3(a)). CHRNA3$^+$ neurons exhibited a similar sodium channel expression profile as NPY2R$^+$ neurons, with higher levels of $Na_v1.6$, $Na_v1.7$, $Na_v1.8$, β2 and β4 than IB4$^-$/caps$^+$ neurons, but none of the differences was statistically significant.

Taken together, our electrophysiological characterization together with the results of the qRT-PCR indicate that each of the three major subsets of TrkA$^+$ nociceptors expresses a different combination of sodium channel α- and β-subunits, which results in the generation of functionally different sodium currents in each of the three subpopulations.

## *NGF differentially modulates VGSC in different subsets of TrkA$^+$ nociceptors*

We next asked if the TTX-S and TTX-R currents are differentially modulated by NGF in the three nociceptor subpopulations. To this end, 100 ng/ml NGF was added to the growth medium at the time of cell plating, and sodium currents were recorded on the next day – i.e.

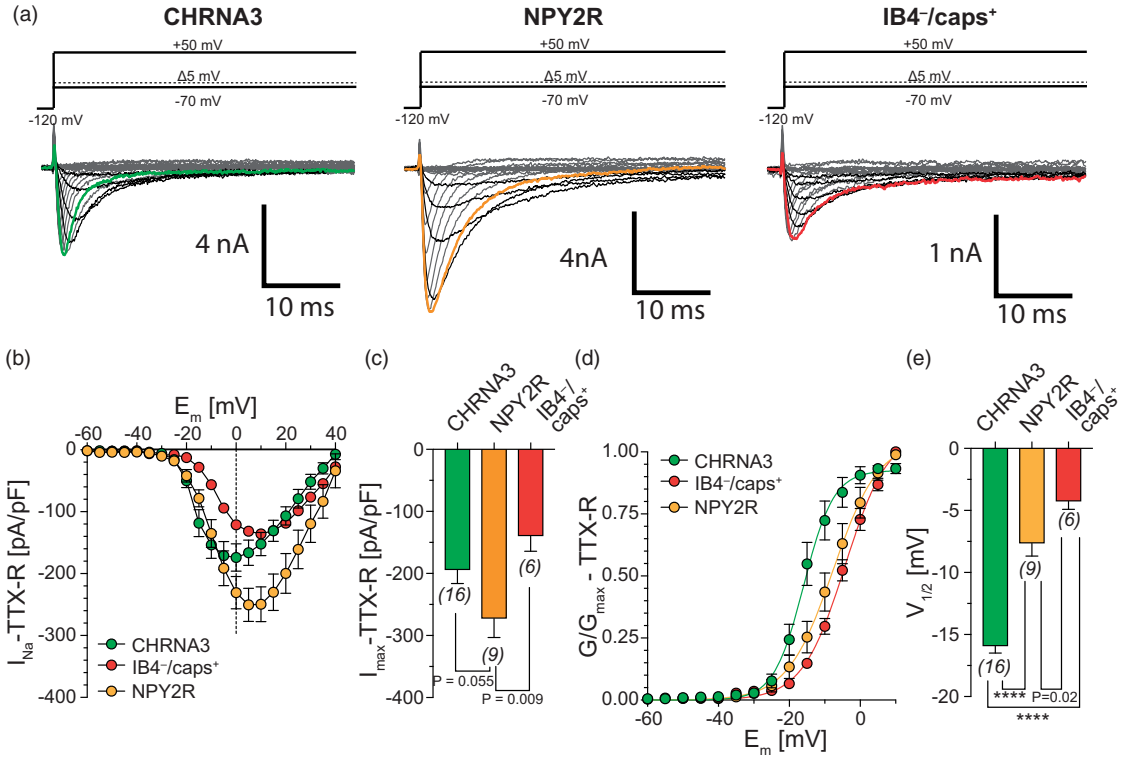


**Figure 2.** Differences in TTX-R sodium currents in three major subsets of TrkA-expressing neurons. (a) Representative example traces of TTX-R currents (bottom traces) elicited by the indicated pulse protocol (top trace). (b) Current–voltage relationship of the TTX-R currents (mean current densities ± SEM) in the indicated cell types. (c) Comparison of the current densities of the maximal TTX-R current in the indicated cell types using one-way ANOVA and Holm-Sidak's multiple comparison test. Note that the current densities of the TTX-R current in NPY2R$^+$ neurons are significantly bigger than in the other two subtypes. (d) Boltzmann fits of the conductance–voltage plots showing that TTX-R currents in NPY2R$^+$ and CHRNA$^+$ activate at more negative potentials compared to TTX-R currents in IB4$^-$ neurons. (g) Comparison of the $V_{1/2} \pm$ SEM values obtained by the Boltzmann fits shown in (f). Boltzmann fits ($V_{1/2}$ values) were compared pairwise using the extra sum-of-squares F-test. ****$P < 0.0001$. TTX: tetrodotoxin; IB4: Isolectin B4; NPY2R: neuropeptide Y receptor type 2; CHRNA3: nicotinic acetylcholine receptor alpha-3 subunit.

usually between 20 and 28 h after the addition of NGF. NGF treatment did not alter any of the examined properties of TTX-S currents in CHRNA3$^+$ neurons (Figure 4(a) to (d)). However, NGF did induce a significant increase in the TTX-R current density in these neurons, from $-188.4 \pm 21.7$ pA/pF under control conditions to $-291.3 \pm 22.2$ pA/pF after NGF treatment (Figure 4(e) to (f)). The half-activation voltage of TTX-R currents was only minimally affected (Figure 4(g) to (h)). Surprisingly, the effects of NGF on NPY2R$^+$ neurons were completely different. Thus, NGF treatment caused a small but significant reduction in the TTX-S current densities (CTL: $-1052 \pm 123.8$ pA/pF vs. NGF: $-694.3 \pm 73.2$ pA/pF; Figure 5(a) and (b)); the voltage dependence of activation of TTX-S current was not altered (TTX-S-CTL-$V_{1/2} = -30.3 \pm 0.4$ mV vs. TTX-S-NGF-$V_{1/2} = -29.4 \pm 0.7$ mV; Figure 5(c) and (d)). Unlike in CHRNA3$^+$ neurons, NGF treatment did not alter the TTX-R current densities in NPY2R$^+$ (Figure 5(e) and (f)) but instead shifted the half-activation voltage by ~7 mV to more negative potentials (TTX-R-CTL-$V_{1/2} = -8.7 \pm 0.7$ mV vs. TTX-R-NGF-$V_{1/2} = -15.1 \pm 1.0$ mV; Figure 5(g) and (h)). The sodium currents in IB4$^-$/caps$^+$ neurons were modulated in a similar manner as those in NPY2R$^+$ neurons. Thus, the TTX-S current densities in IB4$^-$/caps$^+$ neurons were slightly, though not significantly, reduced by NGF treatment (Figure 6(a) and (b)). Interestingly, in contrast to NPY2R$^+$ and CHRNA3$^+$ neurons, NGF treatment significantly shifted the voltage dependence of activation to more negative potentials in IB4$^-$/caps$^+$ neurons (TTX-S-CTL-$V_{1/2} = -13.9 \pm 0.7$ mV vs. TTX-S-NGF-$V_{1/2} = -19.6 \pm 1.3$ mV; Figure 6(c) and (d)). TTX-R current densities were also slightly, but not significantly, increased (Figure 6(e) and (f)) and, as in NPY2R$^+$ neurons, NGF shifted the $V_{1/2}$ of the TTX-R currents in IB4$^-$/caps$^+$ neurons by ~12 mV to more negative potentials (TTX-R-CTL-$V_{1/2} = -3.9 \pm 0.5$ mV vs. TTX-R-NGF-$V_{1/2} = -16.4 \pm 1.3$ mV; Figure 6(g) and (h)). We next asked if the effects of NGF on sodium current properties could, at least partially, be attributed to changes in the expression levels of sodium channel α-

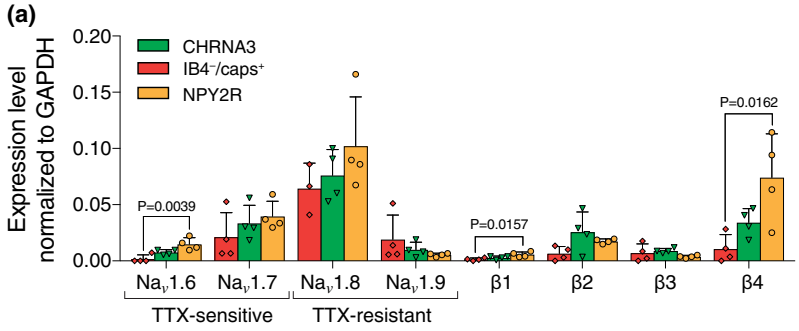


**Figure 3.** Comparison of the expression patterns of sodium channel $\alpha$ and $\beta$ subunits. (a) Bars show the mean ± SEM mRNA expression levels of the indicated sodium channel $\alpha$- and $\beta$-subunits normalized to the expression levels of the housekeeping gene GAPDH in the same samples. The expression levels of the individual samples are indicated by the symbols. The mean expression levels were compared using one-way ANOVA and Holm–Sidak's multiple comparison test and where significant differences were observed, the exact P values are provided in the graph. TTX: tetrodotoxin; GAPDH: Glyceraldehyde 3-phosphate dehydrogenase; IB4: Isolectin B4; NPY2R: neuropeptide Y receptor type 2; CHRNA3: nicotinic acetylcholine receptor alpha-3 subunit.

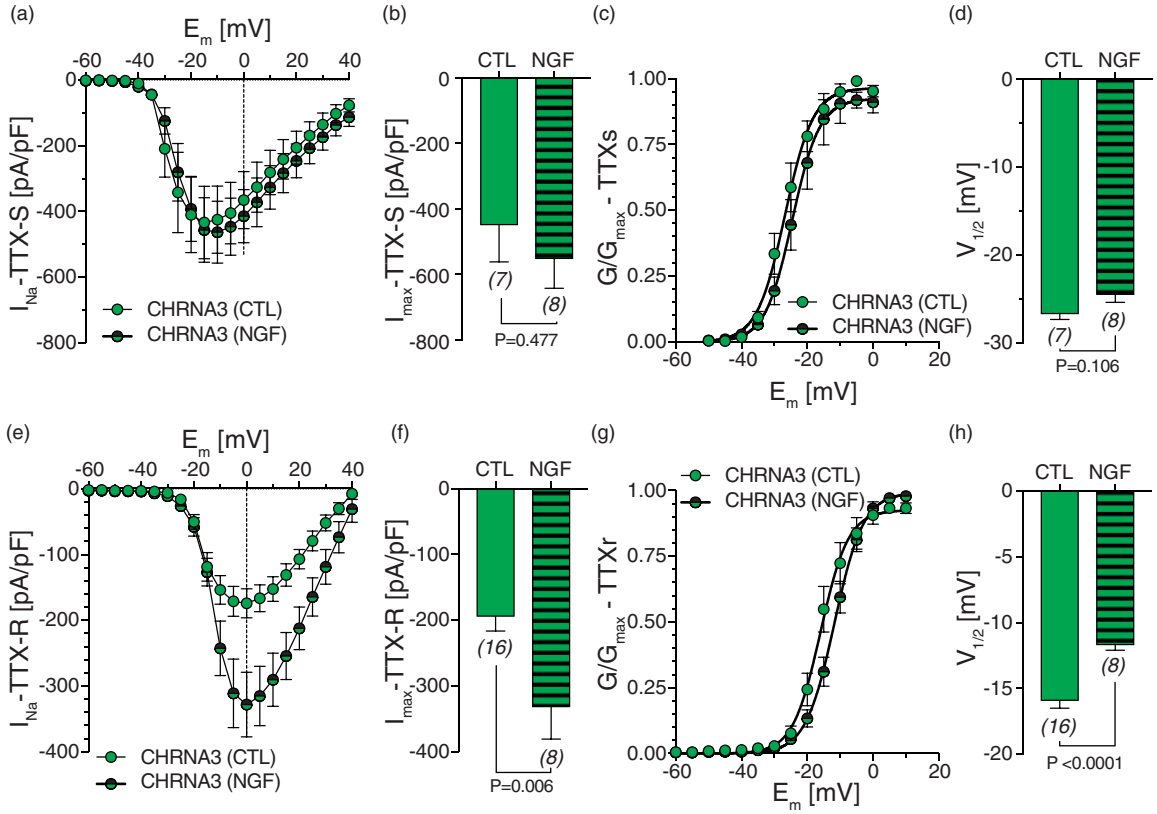


**Figure 4.** Modulation of TTX-S and TTX-R currents by NGF in silent nociceptors. (a) Current–voltage relationship of the TTX-S currents (mean current densities ± SEM) in CHRNA3$^+$ neurons cultured for 24 h in normal growth medium (CTL; green circles) and 24 h in the presence of 100 ng/ml NGF (NGF, half-filled circles). (b) Comparison of the current densities of the maximal TTX-S current in control conditions (CTL, green bars) and in the presence of NGF (hatched bars) using Student's t-test. (c) Boltzmann fits of the conductance–voltage plots showing that NGF does not alter the voltage dependence of activation of TTX-S currents in CHRNA$^+$ neurons. (d) Comparison of the $V_{1/2}$ ± SEM values obtained by the Boltzmann fits shown in (c). Boltzmann fits ($V_{1/2}$ values) were compared using the extra sum-of-squares F-test. (e) Current–voltage relationship of the TTX-R currents (mean current densities ± SEM) in CHRNA3$^+$ neurons. (f) Comparison of the current densities of the maximal TTX-R current using Student's t-test showing that NGF significantly increases the TTX-R current in CHRNA3$^+$ neurons (g) Boltzmann fits of the conductance–voltage plots showing that NGF does not alter the voltage dependence of activation of TTX-R currents in CHRNA$^+$ neurons. (h) Comparison of the $V_{1/2}$ ± SEM values in the absence and presence of NGF obtained by the Boltzmann fits shown in (g). Boltzmann fits ($V_{1/2}$ values) were compared using the extra sum-of-squares F-test. N-numbers were same in (a) to (h) and are provided below the bars in (b), (d), (f), and (h). The exact P values of the statistical comparisons are also indicated below the bar graphs. TTX: tetrodotoxin; CTL: control; NGF: nerve growth factor; CHRNA3: nicotinic acetylcholine receptor alpha-3 subunit.

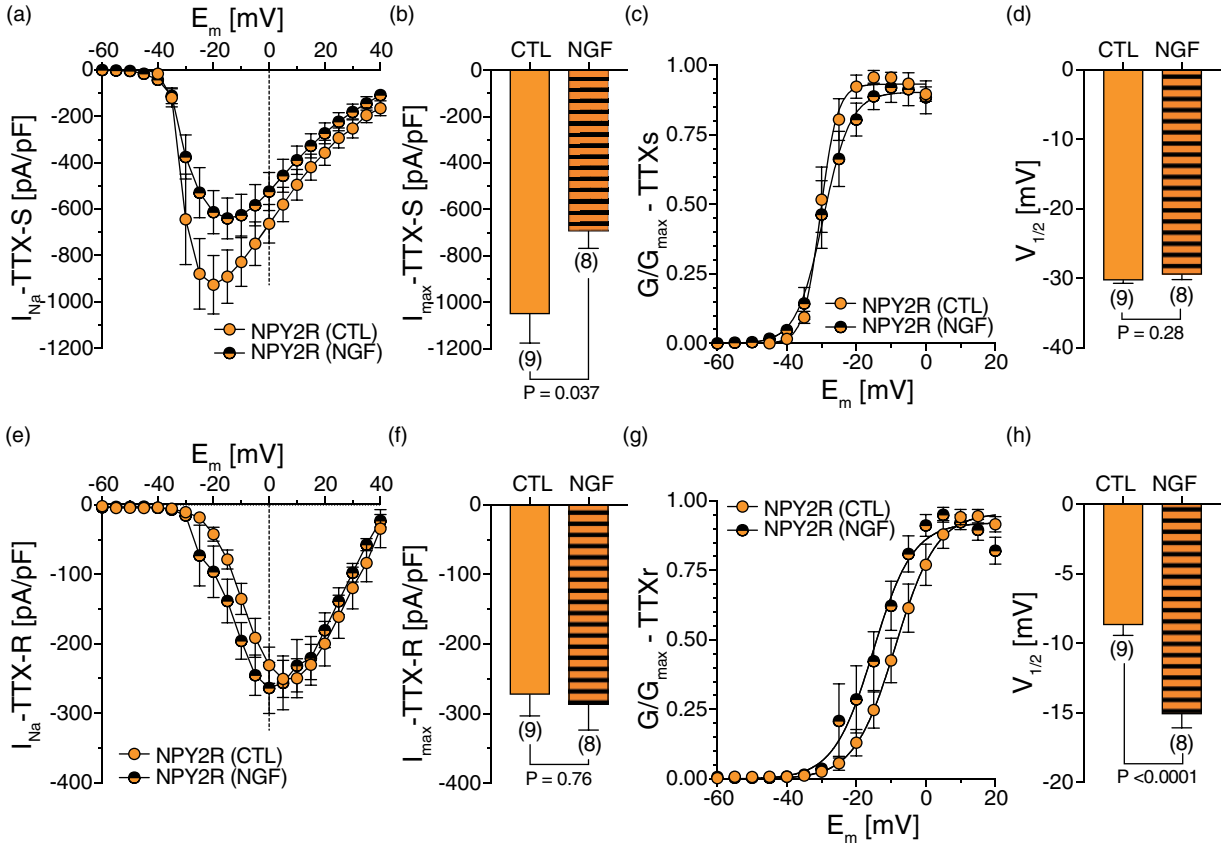


**Figure 5.** Modulation of TTX-S and TTX-R currents by NGF in NPY2R$^+$ A$\delta$-nociceptors. (a) Current–voltage relationship of the TTX-S currents (mean current densities ± SEM) in NPY2R$^+$ neurons cultured for 24 h in normal growth medium (CTL; orange circles) and 24 h in the presence of 100 ng/ml NGF (NGF, half-filled circles). (b) Comparison of the current densities of the maximal TTX-S currents in control conditions (CTL, orange bars) and in the presence of NGF (hatched bars) using Student's t-test showing that NGF causes a small but significant reduction in TTX-S current density. (c) Boltzmann fits of the conductance–voltage plots showing that NGF does not alter the voltage dependence of activation of TTX-S currents in NPY2R$^+$ neurons. (d) Comparison of the $V_{1/2}$ ± SEM values in the absence and presence of NGF obtained by the Boltzmann fits shown in (c) using the extra sum-of-squares F-test. (e) Current–voltage relationship of the TTX-R currents (mean current densities ± SEM) in NPY2R$^+$ neurons. (f) Comparison of the current densities of the maximal TTX-R current using Student's t-test. (g) Boltzmann fits of the conductance–voltage plots showing that NGF shifts the voltage dependence of activation of TTX-R currents in NPY2R$^+$ neurons to more hyperpolarized potentials. (h) Comparison of the $V_{1/2}$ ± SEM values obtained by the Boltzmann fits shown in (g) using the extra sum-of-squares F-test showing that NGF treatment shifts the half-activation voltage by ~7 mV from −8.7 ± 0.7 mV to −15.1 ± 1.0 mV. N-numbers were same in (a) to (h) and are provided below the bars in (b), (d), (f), and (h). The P values of the statistical comparisons are also indicated below the bar graphs. TTX: tetrodotoxin; CTL: control; NGF: nerve growth factor; NPY2R: neuropeptide Y receptor type 2.

and β-subunits. To this end, we compared the mRNA levels of $Na_v1.6$–1.9 and $\beta_{1-4}$ in cells that were cultured for 24 h in normal growth medium with cells that were cultured in the presence of 100 ng/ml NGF for the same period of time. Surprisingly, the only noteworthy change that we could observe was a more than two-fold down-regulation of the mRNA levels of $Na_v1.8$ in IB4$^-$/caps$^+$ neurons, which, however, was not statistically significant (Figure 7(a) to (c)). All other sodium channel α- and β-subunits appeared to be expressed at the same level in the absence and presence of NGF.

Taken together, our results show that NGF differentially modulates voltage-gated sodium currents in different subpopulations of TrkA$^+$ neurons and suggest that none of these effects is mediated by changes in the expression levels sodium channel α- or β-subunits.

## Discussion

The goal of this study was to examine the properties of voltage-gated sodium currents in two recently identified subpopulations of TrkA$^+$ nociceptors, namely, CHRNA3$^+$ 'silent' C-fibre nociceptors[19] and NPY2R$^+$ Aδ-fibre nociceptors[31] and to compare them with the well-characterized sodium channel properties of TrkA$^+$ polymodal C-fibre nociceptors. Moreover, we asked if

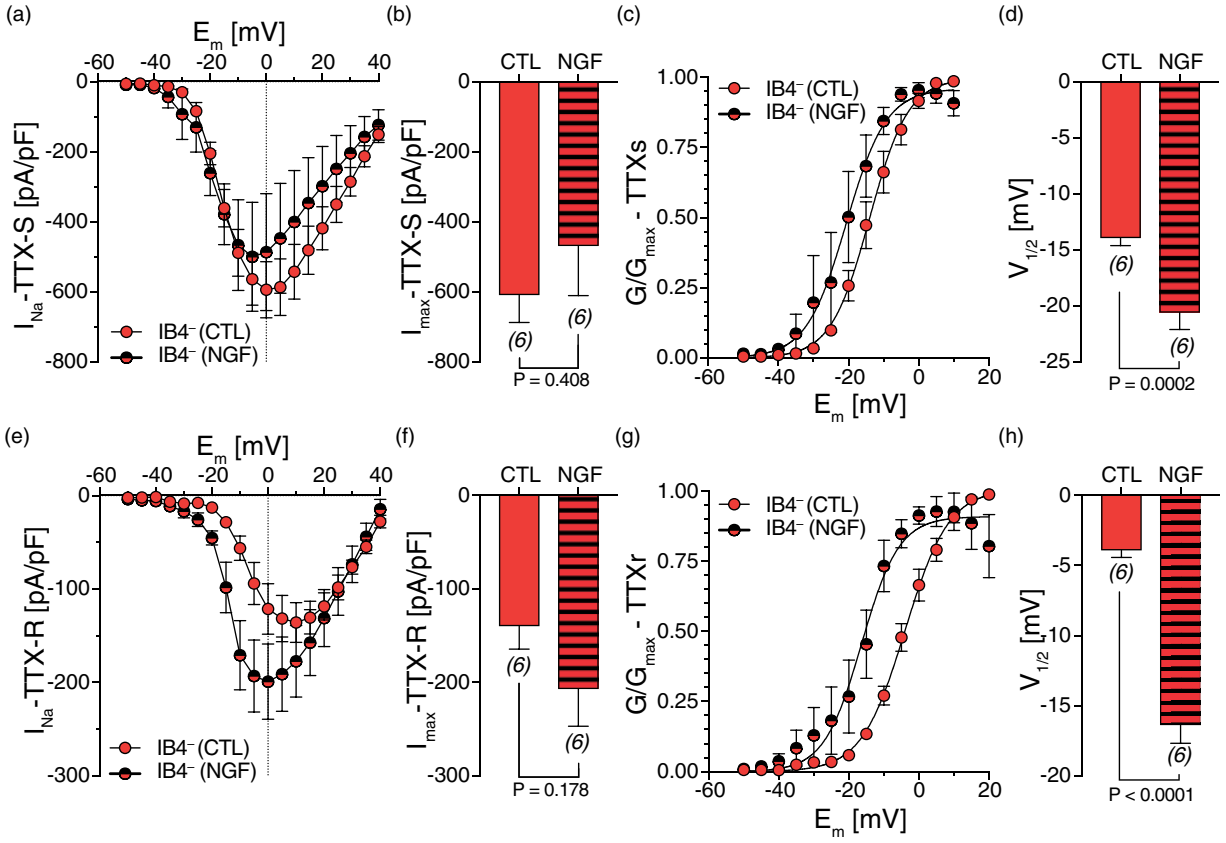


**Figure 6.** Modulation of TTX-S and TTX-R currents by NGF in polymodal C-fibre nociceptors. (a) Current–voltage relationship of the TTX-S currents (mean current densities ± SEM) in small diameter IB4$^-$ capsaicin-sensitive (caps$^+$) neurons cultured for 24 h in normal growth medium (CTL; red circles) and 24 h in the presence of 100 ng/ml NGF (NGF, half-filled circles). (b) Comparison of the current densities of the maximal TTX-S current using Student's t-test showing that NGF does not alter TTX-S current density in IB4$^-$/caps$^+$ neurons. (c) Boltzmann fits of the conductance–voltage plots showing that NGF shifts the voltage dependence of activation of TTX-S currents in IB4$^-$/caps$^+$ neurons to more hyperpolarized potentials. (d) Comparison of the $V_{1/2}$ ± SEM values obtained by the Boltzmann fits shown in (c) using the extra sum-of-squares F-test. Note that NGF treatment shifts the half-activation voltage by ~6 mV from −13.9 ± 0.7 mV to −19.6 ± 1.3 mV. (e) Current–voltage relationship of the TTX-R currents (mean current densities ± SEM) in the same cells shown in (a) to (d). (f) Comparison of the current densities of the maximal TTX-R current using Student's t-test. (g) Boltzmann fits of the conductance–voltage plots showing that NGF shifts the voltage dependence of activation of TTX-R currents in IB4$^-$/caps$^+$ neurons to more hyperpolarized potentials. (h) Comparison of the $V_{1/2}$ ± SEM values obtained by the Boltzmann fits shown in (g) using the extra sum-of-squares F-test showing that NGF treatment shifts the half-activation voltage by ~12 mV from −3.9 ± 0.5 mV to −16.4 ± 1.3 mV. N-numbers were same in (a) to (h) and are provided below the bars in (b), (d), (f), and (h). The P values of the statistical comparisons are also indicated below the bar graphs. TTX: tetrodotoxin; CTL: control; NGF: nerve growth factor; IB4: Isolectin B4.

the inflammatory mediator NGF exerts different effects on VGSCs in these three nociceptor subpopulations. Indeed, we observed significant differences in the properties of voltage-gated sodium currents and found that NGF differentially modulates sodium currents in the three cell types.

In summary, we made the following observations:

(i) TTX-S and TTX-R sodium currents in CHRNA3$^+$ and NPY2R$^+$ neurons are activated at more negative potentials than TTX-S currents in IB4$^-$/caps$^+$ neurons, which correlates with the different expression levels of $\beta$1 and $\beta$4 subunits in these cell types.

(ii) NPY2R$^+$ neurons have significantly higher TTX-R current densities than CHNRA3$^+$ and IB4$^-$/caps$^+$ neurons.

(iii) We observed that NGF shifts the half-activation voltage of TTX-R currents to more negative potentials in NPY2R$^+$ and IB4$^-$/caps$^+$ neurons, but not in CHRNA3$^+$ neurons, whereas it increased current densities of TTX-R current only in CHRNA3$^+$ and to a smaller extent in IB4$^-$/caps$^+$ neurons.

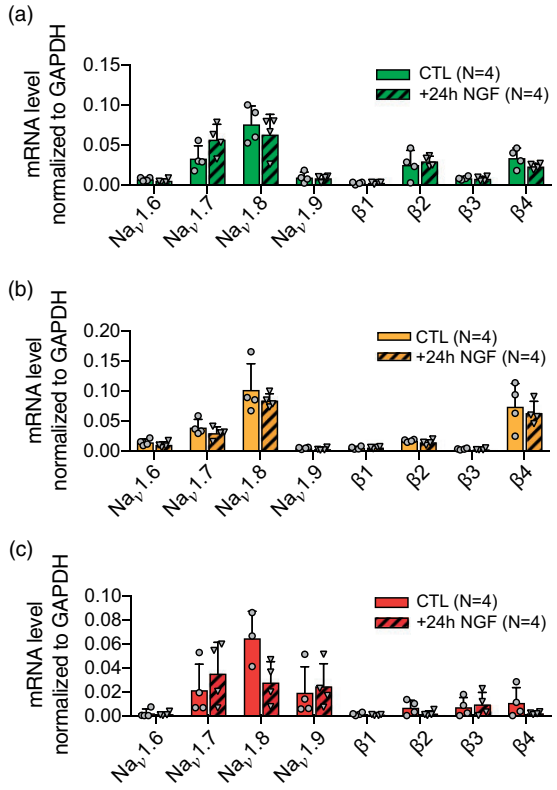


**Figure 7.** NGF does not alter the expression levels of sodium channel $\alpha$- and $\beta$-subunits. Comparisons of the mean ± SEM mRNA expression levels of the indicated sodium channel $\alpha$- and $\beta$-subunits normalized to the expression levels of the housekeeping gene GAPDH in CHRNA3$^+$ (a), NPY2R$^+$ (b) and IB4$^-$/caps$^+$ (c) neurons cultured for 24 h in the absence (CTL) and neurons cultured for 24 h in the presence of 100 ng/ml NGF (NGF). The expression levels of the individual samples are indicated by the symbols. The expression levels were compared using Student's t-test, but no significant changes in mRNA expression were detected. GAPDH: Glyceraldehyde 3-phosphate dehydrogenase; CTL: control; NGF: nerve growth factor.

(iv) We demonstrate that NGF shifts the half-activation voltage of TTX-S currents to more negative potentials in IB4$^-$/caps$^+$ neurons but not in CHRNA3$^+$ and NPY2R$^+$ neurons, whereas it reduces the current density of TTX-S currents in NPY2R$^+$ neurons and to a small though not significant extent in IB4$^-$/caps$^+$ neurons.

### *Differences in the expression levels of sodium channel α- and β-subunits account for the functional differences in sodium current in the three nociceptor subpopulation*

One of the key findings of this study was that TTX-S currents in CHRNA3$^+$ and NPY2R$^+$ nociceptors are activated at more negative potentials than TTX-S currents in IB4$^-$/caps$^+$ nociceptors (Figure 1(c) to (g)). One possible explanation for these differences is that the former two subpopulations express significant amounts of Na$_v$1.6 and the β4-subunit (Figure 3). Na$_v$1.6 has been shown to be activated at rather negative potentials, though it should be noted that the reported $V_{1/2}$ values of Na$_v$1.6 in DRG neurons vary between −35.9 mV and −18.7 mV in different studies,[34,35] and the β4-subunit was previously shown to shift the half-activation voltage of Na$_v$1.6 by ∼8 mV to hyperpolarized potentials in heterologous systems.[36] Hence, the co-expression of these two proteins is most likely the reason for the extremely hyperpolarized half-activation voltages of TTX-S current in NPY2R$^+$ and CHRNA3$^+$ neurons. Our observation that NPY2R$^+$ neurons, which are Aδ-fibre nociceptors, express high levels of Na$_v$1.6 is consistent with previous reports showing that myelinated Aδ- and Aβ-fibres but not C-fibre nociceptors express Na$_v$1.6.[37,38] We are not aware of any study that has examined the expression of Na$_v$1.6 in silent nociceptors, but recently Feng et al.[39] demonstrated Nav1.6 expression in a significant proportion of Nav1.8-expressing colorectal afferents. Considering that CHRNA3$^+$ afferents account for approximately one half of all nociceptive peptidergic colorectal afferents,[19] it is tempting to speculate that these fibres were also included in the population labelled by Feng et al.[39] For Na$_v$1.7, $V_{1/2}$ values around −25 mV have previously been reported[35,40] and there is no evidence suggesting that β-subunits alter the voltage dependence of Na$_v$1.7 activation.[40–42] However, phosphorylation by ERK1/2 was shown to shift the $V_{1/2}$ of Na$_v$1.7 to more negative potentials.[30] Hence, another possible explanation for the hyperpolarized half-activation voltages is that the basal activity of ERK1/2 is higher in NPY2R$^+$ and CHRNA3$^+$ neurons.

Another important observation of our study was that the TTX-R currents in NPY2R$^+$ neurons had significantly higher current densities than CHRNA3$^+$ neurons and IB4$^-$/caps$^+$ neurons (Figure 2(c)). Since NPY2R$^+$ neurons only express small amounts of Na$_v$1.9 (Figure 3), most of the TTX-R current is probably carried by Na$_v$1.8. The expression levels of Na$_v$1.8 did not significantly differ between the three populations (Figure 3) and thus we propose that the high TTX-R current densities in NPY2R$^+$ neurons result from the significantly higher levels of the β1-subunit (Figure 3), which has indeed been shown to increase Na$_v$1.8 mediated currents in heterologous systems.[36] We further observed that TTX-R currents in CHRNA3$^+$ neurons had more hyperpolarized half-activation voltages than TTX-R currents in both NPY2R$^+$ and IB4$^-$/caps$^+$ nociceptors (Figure 2). The hyperpolarized half-activation voltage of TTX-R currents in CHRNA3$^+$ is consistent with the high expression levels of the β4-subunit, which was shown to shift the $V_{1/2}$ of Na$_v$1.8 to hyperpolarized potentials by more than 15 mV,[36] which is comparable

to the difference between CHRNA3$^+$ and IB4$^-$/caps$^+$ positive observed here (Figure 2(d) and (e)). Cell-to-cell variability in the properties of TTX-R sodium currents has previously been reported,[43] and, moreover, it was shown that modulation of $Na_v$ channel function by β-subunits can depend on the cellular background. The β1-subunit, for example, was shown to increase the rate of open-channel inactivation and to shift steady-state inactivation of Nav1.3 in Xenopus oocytes but not in HE293 cells.[44] Sodium channel function is also altered by posttranslational modifications, e.g. by protein kinases, glycosylation and ubiquitylation.[20,21] Hence, one possible explanation for the cell type-specific effects of β-subunits is that different posttranslational modifications occur in different cell types, which could also explain why TTX-R currents in NPY2R$^+$ neurons have half-activation voltages similar to TTX-R currents in IB4$^-$/caps$^+$ neurons (Figure 2(d) and (e)), despite expressing significantly higher levels of the β4 subunit (Figure 3). However, considering the variety of possible post-translational modification of VGSCs that had previously been described in other cells types,[20,21] we did not address this question here, as this would have been beyond the scope of this study.

### *NGF differentially modulates sodium currents in different subsets of TrkA$^+$ nociceptors*

The second major goal of our study was to test if NGF, which has previously been shown to modulate sodium currents in small diameter IB4$^-$ capsaicin-sensitive nociceptors, also modulates sodium currents in silent nociceptors (CHRNA3$^+$) and Aδ-fibre nociceptors (NPY2R$^+$). Specifically, we focused on two parameters – i.e. current density and voltage dependence of activation. Regarding current densities, our data show that NGF induces a significant increase in TTX-R currents in CHRNA3$^+$ neurons (Figure 4(f)) but not in NPY2R$^+$ neurons (Figure 5(f)), while it causes a small but significant decrease in TTX-S current density in NPY2R$^+$ neurons (Figure 5(b)) without affecting TTX-S currents in CHRNA3$^+$ nociceptors (Figure 4(b)). As mentioned earlier, changes in the current densities might result from changes in the expression levels of α-subunits and/or β-subunits, some of which are well known to enhance membrane trafficking of sodium channels.[20,41] However, unlike previously reported for small diameter neuron in long-term DRG cultures (7 div),[45] we did not observe an up-regulation of $Na_v1.8$ in CHRNA3$^+$ neurons (Figure 7(a)) after 24 h NGF treatment. Moreover, we neither detected a down-regulation of $Na_v1.7$ in NPY2R$^+$ neurons (Figure 7(b)) nor any significant changes in β-subunit expression in these two nociceptor subpopulations, suggesting that the changes in current densities are probably induced by post-translational modifications rather than transcriptional changes. In fact, downstream effectors of NGF-TrkA signalling, including p38 MAP kinase and ceramide, have previously been shown to increase $Na_v1.8$ currents in small diameter IB4$^-$/caps$^+$ neurons, in case of p38 by facilitating membrane trafficking.[22,23,46] We also observed the previously described NGF-induced increase in Nav1.8 amplitudes in small diameter IB4$^-$/caps$^+$ neurons, though in our hands, this effect was not statistically significant, which may be attributed to the rather small samples size of these cells in our study (Figure 6(e) and (f)). The reduction in TTX-S current density in NPY2R$^+$ neurons was significant, but rather small (Figure 5(b)), and was not reflected in a downregulation of TTX-S sodium channel α- or β-subunits (Figure 7(b)). However, the cell capacitance of NPY2R$^+$ neurons increased from $30.5 \pm 1.7$ pF to $46.2 \pm 5.3$ pF after NGF treatment, which provides an alternative explanation for this effect.

The most robust effects of NGF on sodium currents that we observed were the hyperpolarizing shifts of the half-activation voltages of TTX-R currents in NPY2R$^+$ (Figure 5(g) and (h)) and IB4$^-$/caps$^+$ neurons (Figure 6 (g) and (h)) and the hyperpolarizing shift in $V_{1/2}$ of TTX-S currents in IB4$^-$/caps$^+$ neurons (Figure 6(c) and (d)). It is difficult to unequivocally attribute changes in TTX-S and TTX-R currents to changes in the functional properties of a single sodium channel, because these are composite currents generated from multiple channels.[47] This is particularly true for the TTX-S currents in CHRNA3$^+$ and NPY2R$^+$ neurons, which express both $Na_v1.6$ and $Na_v1.7$ at considerable levels (Figure 3). The TTX-R currents are, however, most likely predominantly generated by Nav1.8, which is expressed at much higher levels than Nav1.9 in all three studied nociceptor populations (Figure 3). An NGF-induced hyperpolarizing shift in the voltage dependence of TTX-R sodium current, which is thought to be mediated by second messenger ceramide-induced activation of PKCζ, has previously been reported for small diameter IB4$^-$/caps$^+$ neurons,[23,24] but it has never been tested if this effect also occurs in other TrkA$^+$ nociceptors. We did not detect any significant changes in the expression of sodium channel α-subunits and β-subunits (Figure 7 (b)), which can also change the voltage dependence of activation.[20,41] Hence, it is tempting to speculate that the NGF-induced hyperpolarizing shift in the $V_{1/2}$ of TTX-R currents in NPY2R$^+$ Aδ-nociceptors may be mediated by the same mechanisms that was previously described for IB4$^-$/caps$^+$ neurons.[23,24] Since NGF is known to activate ERK1/2 MAP kinases[1,48] and phosphorylation of $Na_v1.7$ by ERK1/2 was shown to cause a hyperpolarizing shift of channel activation,[30] it has been hypothesized that NGF shifts the $V_{1/2}$ of TTX-S currents to more negative potentials, but actually this hypothesis

has never been directly tested. Here, we demonstrate that NGF indeed shifts the voltage dependence of the TTX-S current in small diameter $IB4^-/caps^+$ neurons as previously proposed but not in myelinated $NPY2R^+$ Aδ-fibre nociceptors or $CHRNA3^+$ silent nociceptors. The observation that NGF did not alter the voltage dependence of activation of TTX-S currents in $NPY2R^+$ and $CHRNA3^+$ neurons was quite unexpected considering that ERK1/2, which supposedly mediates this effect in $IB4^-/caps^+$ neurons, is also activated by NGF in $CHRNA3^+$ neurons, as we have recently shown,[19] and probably also in $NPY2R^+$ neurons. While we can only speculate about the possible reasons for the lack of TTX-S sodium current modulation in $CHRNA3^+$ neurons, our results clearly demonstrate that NGF exerts different effects on different nociceptor subpopulations, even though these subpopulations appear to express the same downstream effector proteins.

## Conclusions

Previous studies have shown that each of the three subpopulations of nociceptors examined here is important for different forms of pain. Thus, $NPY2R^+$ Aδ-fibre are required for pinprick pain,[31] whereas $IB4^-/caps^+$ C-fibre nociceptors signal heat pain and detect painful pinch stimuli,[16,49] and $CHRNA3^+$ silent nociceptors are the most abundant $TrkA^+$ nociceptors innervating visceral organs and deep somatic tissues.[19] Hence, our observation that NGF exerts different effects on sodium currents in Aδ-fibre nociceptors and polymodal C-fibre nociceptors as compared to silent nociceptors indicates that visceral and cutaneous pain may be mediated by fundamentally different mechanisms and thus highlights the importance of developing different therapeutic strategies for different forms of pain. We have not examined which downstream effectors of TrkA mediate the different effects of NGF on sodium currents in $CHRNA3^+$ and $NPY2R^+$ neurons as this would have been beyond the scope of this study, but our work provides a solid basis for future studies that aim at addressing this important question.

### Acknowledgements

The authors would like to thank Ms. Paulina Schad and Ms. Anke Niemann for technical assistance.

### Author Contributions

IS was involved in investigation and writing; VP, AA and FJT were involved in investigation; SGL contributed to writing, conceptualization, methodology, funding acquisition, resources and supervision.

### Declaration of Conflicting Interests

The author(s) declared no potential conflicts of interest with respect to the research, authorship, and/or publication of this article.

### Funding

The author(s) disclosed receipt of the following financial support for the research, authorship, and/or publication of this article: This work was funded by Deutsche Forschungsgemeinschaft (DFG) grants #LE3210/1–2 and SFB1158/1 to S.G.L.

### References

1. Denk F, Bennett DL and McMahon SB. Nerve growth factor and pain mechanisms. *Annu Rev Neurosci* 2017;40: 307–325.
2. Lewin GR, Lechner SG and Smith ESJ. Nerve growth factor and nociception: from experimental embryology to new analgesic therapy. *Handb Exp Pharmacol* 2014; 220: 251–282.
3. Chen W, Ye D-Y, Han D-J, Fu G-Q, Zeng X and Lin W. Elevated level of nerve growth factor in the bladder pain syndrome/interstitial cystitis: a meta-analysis. *SpringerPlus* 2016; 5: 1072.
4. di Mola FF, Friess H, Zhu ZW, Koliopanos A, Bley T, Di Sebastiano P, Innocenti P, Zimmermann A and Büchler MW. Nerve growth factor and Trk high affinity receptor (TrkA) gene expression in inflammatory bowel disease. *Gut* 2000; 46: 670–679.
5. Friess H, Zhu ZW, di Mola FF, Kulli C, Graber HU, Andren-Sandberg A, Zimmermann A, Korc M, Reinshagen M and Büchler MW. Nerve growth factor and its high-affinity receptor in chronic pancreatitis. *Ann Surg* 1999; 230: 615–624.
6. Iannone F, De BC, Dell'Accio F, Covelli M, Patella V and Lo BG. Increased expression of nerve growth factor (NGF) and high affinity NGF receptor (p140 TrkA) in human osteoarthritic chondrocytes. *Rheumatol Oxf Engl* 2002; 41: 1413–1418.
7. Dyck PJ, Peroutka S, Rask C, Burton E, Baker MK, Lehman KA, Gillen DA, Hokanson JL and O'Brien PC. Intradermal recombinant human nerve growth factor induces pressure allodynia and lowered heat-pain threshold in humans. *Neurology* 1997; 48: 501–505.
8. Rukwied R, Mayer A, Kluschina O, Obreja O, Schley M and Schmelz M. NGF induces non-inflammatory localized and lasting mechanical and thermal hypersensitivity in human skin. *Pain* 2010; 148: 407–413.
9. Hirth M, Rukwied R, Gromann A, Turnquist B, Weinkauf B, Francke K, Albrecht P, Rice F, Hägglöf B, Ringkamp M, Engelhardt M, Schultz C, Schmelz M and Obreja O. Nerve growth factor induces sensitization of nociceptors without evidence for increased intraepidermal nerve fiber density. *Pain* 2013; 154: 2500–2511.
10. Lewin GR, Ritter AM and Mendell LM. Nerve growth factor-induced hyperalgesia in the neonatal and adult rat. *J Neurosci* 1993; 13: 2136–2148.

11. Mills CD, Nguyen T, Tanga FY, Zhong C, Gauvin DM, Mikusa J, Gomez EJ, Salyers AK and Bannon AW. Characterization of nerve growth factor-induced mechanical and thermal hypersensitivity in rats. *Eur J Pain* 2013; 17: 469–479.
12. Woolf CJ, Safieh-Garabedian B, Ma QP, Crilly P and Winter J. Nerve growth factor contributes to the generation of inflammatory sensory hypersensitivity. *Neuroscience* 1994; 62: 327–331.
13. Chang DS, Hsu E, Hottinger DG and Cohen SP. Anti-nerve growth factor in pain management: current evidence. *J Pain Res* 2016; 9: 373–383.
14. Vay L, Gu C and McNaughton PA. The thermo-TRP ion channel family: properties and therapeutic implications. *Br J Pharmacol* 2012; 165: 787–801.
15. Caterina MJ, Leffler A, Malmberg AB, Martin WJ, Trafton J, Petersen-Zeitz KR, Koltzenburg M, Basbaum AI and Julius D. Impaired nociception and pain sensation in mice lacking the capsaicin receptor. *Science* 2000; 288: 306–313.
16. Brenneis C, Kistner K, Puopolo M, Segal D, Roberson D, Sisignano M, Labocha S, Ferreirós N, Strominger A, Cobos EJ, Ghasemlou N, Geisslinger G, Reeh PW, Bean BP and Woolf CJ. Phenotyping the function of TRPV1-expressing sensory neurons by targeted axonal silencing. *J Neurosci* 2013; 33: 315–326.
17. Pezet S and McMahon SB. Neurotrophins: mediators and modulators of pain. *Annu Rev Neurosci* 2006; 29: 507–538.
18. Di Castro A, Drew LJ, Wood JN and Cesare P. Modulation of sensory neuron mechanotransduction by PKC- and nerve growth factor-dependent pathways. *Proc Natl Acad Sci U S A* 2006; 103: 4699–4704.
19. Prato V, Taberner FJ, Hockley JRF, Callejo G, Arcourt A, Tazir B, Hammer L, Schad P, Heppenstall PA, Smith ES and Lechner SG. Functional and molecular characterization of mechanoinsensitive "silent" nociceptors. *Cell Rep* 2017; 21: 3102–3115.
20. Laedermann CJ, Abriel H and Decosterd I. Post-translational modifications of voltage-gated sodium channels in chronic pain syndromes. *Front Pharmacol* 2015; 6: 263.
21. Dib-Hajj SD, Cummins TR, Black JA and Waxman SG. Sodium channels in normal and pathological pain. *Annu Rev Neurosci* 2010; 33: 325–347.
22. Hudmon A, Choi J-S, Tyrrell L, Black JA, Rush AM, Waxman SG and Dib-Hajj SD. Phosphorylation of sodium channel Nav1.8 by p38 mitogen-activated protein kinase increases current density in dorsal root ganglion neurons. *J Neurosci* 2008; 28: 3190–3201.
23. Zhang YH, Vasko MR and Nicol GD. Ceramide, a putative second messenger for nerve growth factor, modulates the TTX-resistant Na(+) current and delayed rectifier K (+) current in rat sensory neurons. *J Physiol (Lond)* 2002; 544: 385–402.
24. Zhang YH, Kays J, Hodgdon KE, Sacktor TC and Nicol GD. Nerve growth factor enhances the excitability of rat sensory neurons through activation of the atypical protein kinase C isoform, PKM zeta. *J Neurophysiol* 2012; 107: 315–335.
25. Leffler A, Cummins TR, Dib-Hajj SD, Hormuzdiar WN, Black JA and Waxman SG. GDNF and NGF reverse changes in repriming of TTX-sensitive $Na^+$ currents following axotomy of dorsal root ganglion neurons. *J Neurophysiol* 2002; 88: 650–658.
26. Dib-Hajj SD, Black JA, Cummins TR, Kenney AM, Kocsis JD and Waxman SG. Rescue of α-SNS sodium channel expression in small dorsal root ganglion neurons after axotomy by nerve growth factor in vivo. *J Neurophysiol* 1998; 79: 2668–2676.
27. Fjell J, Cummins TR, Fried K, Black JA and Waxman SG. In vivo NGF deprivation reduces SNS expression and TTX-R sodium currents in IB4-negative DRG neurons. *J Neurophysiol* 1999; 81: 803–810.
28. Okuse K, Chaplan SR, McMahon SB, Luo ZD, Calcutt NA, Scott BP, Akopian AN and Wood JN. Regulation of expression of the sensory neuron-specific sodium channel SNS in inflammatory and neuropathic pain. *Mol Cell Neurosci* 1997; 10: 196–207.
29. Gould HJ, Gould TN, England JD, Paul D, Liu ZP and Levinson SR. A possible role for nerve growth factor in the augmentation of sodium channels in models of chronic pain. *Brain Res* 2000; 854: 19–29.
30. Stamboulian S, Choi J-S, Ahn H-S, Chang Y-W, Tyrrell L, Black JA, Waxman SG and Dib-Hajj SD. ERK1/2 mitogen-activated protein kinase phosphorylates sodium channel Nav1.7 and alters its gating properties. *J Neurosci* 2010; 30: 1637–1647.
31. Arcourt A, Gorham L, Dhandapani R, Prato V, Taberner FJ, Wende H, Gangadharan V, Birchmeier C, Heppenstall PA and Lechner SG. Touch receptor-derived sensory information alleviates acute pain signaling and fine-tunes nociceptive reflex coordination. *Neuron* 2017; 93: 179–193.
32. Mogil JS. Sex differences in pain and pain inhibition: multiple explanations of a controversial phenomenon. *Nat Rev Neurosci* 2012; 13: 859–866.
33. Weyer AD, Zappia KJ, Garrison SR, O'Hara CL, Dodge AK and Stucky CL. Nociceptor sensitization depends on age and pain chronicity. *eNeuro* 2016; 3.
34. Rush AM, Dib-Hajj SD and Waxman SG. Electrophysiological properties of two axonal sodium channels, Nav1.2 and Nav1.6, expressed in mouse spinal sensory neurones. *J Physiol (Lond)* 2005; 564: 803–815.
35. Herzog RI, Cummins TR, Ghassemi F, Dib-Hajj SD and Waxman SG. Distinct repriming and closed-state inactivation kinetics of Nav1.6 and Nav1.7 sodium channels in mouse spinal sensory neurons. *J Physiol (Lond)* 2003; 551: 741–750.
36. Zhao J, O'Leary ME and Chahine M. Regulation of Nav1.6 and Nav1.8 peripheral nerve Na+ channels by auxiliary β-subunits. *J Neurophysiol* 2011; 106: 608–619.
37. Ho C and O'Leary ME. Single-cell analysis of sodium channel expression in dorsal root ganglion neurons. *Mol Cell Neurosci* 2011; 46: 159–166.
38. Fukuoka T and Noguchi K. Comparative study of voltage-gated sodium channel α-subunits in non-overlapping four neuronal populations in the rat dorsal root ganglion. *Neurosci Res* 2011; 70: 164–171.
39. Feng B, Zhu Y, La J-H, Wills ZP and Gebhart GF. Experimental and computational evidence for an essential

role of NaV1.6 in spike initiation at stretch-sensitive colorectal afferent endings. *J Neurophysiol* 2015; 113: 2618–2634.
40. Vijayaragavan K, O'Leary ME and Chahine M. Gating Properties of Nav1.7 and Nav1.8 Peripheral Nerve Sodium Channels. *J Neurosci* 2001; 21: 7909–7918.
41. Brackenbury WJ and Isom LL. Na channel $\beta$ subunits: overachievers of the ion channel family. *Front Pharmacol* 2011; 2: 53.
42. Sokolov MV, Henrich-Noack P, Raynoschek C, Franzén B, Larsson O and Main M. Co-expression of $\beta$ Subunits with the Voltage-Gated Sodium Channel $Na_{V1.7}$: the importance of subunit association and phosphorylation and their effects on channel pharmacology and biophysics. *J Mol Neurosci* 2018; 65: 154–166.
43. Rizzo MA, Kocsis JD and Waxman SG. Slow sodium conductances of dorsal root ganglion neurons: intraneuronal homogeneity and interneuronal heterogeneity. *J Neurophysiol* 1994; 72: 2796–2815.
44. Cummins TR, Aglieco F, Renganathan M, Herzog RI, Dib-Hajj SD and Waxman SG. Nav1.3 sodium channels: rapid repriming and slow closed-state inactivation display quantitative differences after expression in a mammalian cell line and in spinal sensory neurons. *J Neurosci* 2001; 21: 5952–5961.
45. Black JA, Langworthy K, Hinson AW, Dib-Hajj SD and Waxman SG. NGF has opposing effects on Na+ channel III and SNS gene expression in spinal sensory neurons. *NeuroReport* 1997; 8: 2331.
46. Ji R-R, Samad TA, Jin S-X, Schmoll R and Woolf CJ. p38 MAPK activation by NGF in primary sensory neurons after inflammation increases TRPV1 levels and maintains heat hyperalgesia. *Neuron* 2002; 36: 57–68.
47. Cummins TR and Waxman SG. Downregulation of tetrodotoxin-resistant sodium currents and upregulation of a rapidly repriming tetrodotoxin-sensitive sodium current in small spinal sensory neurons after nerve injury. *J Neurosci* 1997; 17: 3503–3514.
48. Teng KK and Hempstead BL. Neurotrophins and their receptors: signaling trios in complex biological systems. *Cell Mol Life Sci* 2004; 61: 35–48.
49. Cavanaugh DJ, Lee H, Lo L, Shields SD, Zylka MJ, Basbaum AI and Anderson DJ. Distinct subsets of unmyelinated primary sensory fibers mediate behavioral responses to noxious thermal and mechanical stimuli. *Proc Natl Acad Sci U S A* 2009; 106: 9075–9080.